Diagnosis of Rotor Faults in Brushless DC (BLDC) Motors Operating Under Non-Stationary Conditions Using Windowed Fourier Ridges

Satish Rajagopalan Thomas G. Habetler
Ronald G. Harley
School of Electrical and Computer Engineering
Georgia Institute of Technology
Atlanta GA 30332-0250 USA
thabetler@ece.gatech.edu

José M. Aller José A. Restrepo

Universidad Simón Bolívar
Caracas 1080A, VENEZUELA
jaller@usb.ve

***Abstract* — There are several applications where the motor is operating in continuous non-stationary operating conditions. Actuators in the aerospace and transportation industries are examples of this kind of operation. Diagnostics of faults in such applications is, however, challenging. A novel method using windowed Fourier ridges is proposed in this paper for the detection of rotor faults in BLDC motors operating under continuous non-stationarity. Experimental results are presented to validate the concept and depict the ability of the proposed algorithm to track and identify rotor faults. The proposed algorithm is simple and can be implemented in real-time without much computational burden.**

Keywords- Electric machines, condition-monitoring, eccentricity, spectrogram, rotor faults

I. INTRODUCTION

In many applications, the electric motor operates under operating conditions (speed and load) that are constantly changing with time. Such applications are commonly encountered in the aerospace, appliances and automotive industries. Diagnosis of motor health in such applications could be critical to maintaining and improving process uptimes in industries or providing increased safety to humans. While diagnostics of faults in motors operating under steady state conditions is straight forward due to the use of the well known Fourier transformation [1-3], diagnostics of motors operating under non-stationary conditions may need more sophisticated signal processing. Often, assumptions of local or slow stationarity may have to be made. Even under these assumptions it is difficult to arrive at a solution that may be effective over a wide range of operating conditions and faults. A typical segment of a permanent magnet brushless DC motor (BLDC) stator current in a non-stationary state is shown in Fig. 1. Here both the frequency and amplitude are changing continuously.

There has been little research in the area of fault diagnostics of motors operating under non-stationary conditions and what has been reported is limited to induction motor applications. Short Time Fourier Transforms (STFT) and statistical methods have been used to detect broken bar and bearing defects from the induction motor stator current in applications where the motor speed and load are constant over sufficient intervals of time during which a Fourier transform could be applied [4]. Wavelet packet transforms and artificial neural networks have also been applied to detect motor faults in similar applications [5]. Some researchers have tried to detect motor faults in induction motors by analyzing the starting current transient [6, 7]. This enables the detection of faults under no load condition where the only measurable and useful information exists in the large starting transient current of the motor. However, nothing has been published that attempts to diagnose faults in applications where the motor is continuously in a non-stationary state or where assumptions of local or slow stationarity may be questionable and unrealistic.

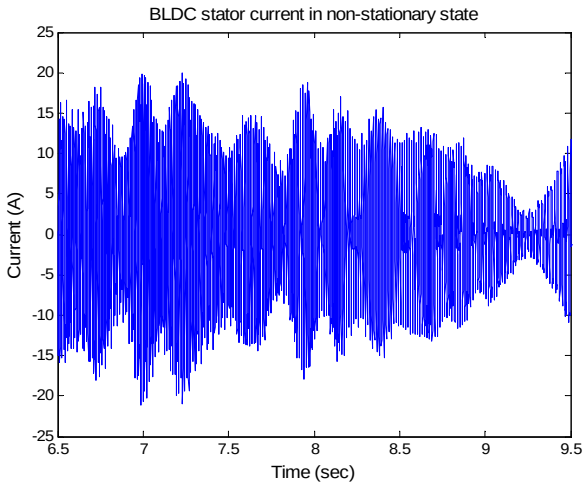

Figure 1. Non-stationary stator current in a BLDC motor.

A windowed Fourier ridge algorithm is proposed in this paper in an attempt to solve this problem. The algorithm computes local maxima (or ridges) from the spectrogram of an adaptively filtered non-stationary motor current signal. The proposed method allows continuous real-time tracking of rotor faults in BLDC motors operating under continuous non-

stationary conditions, thus allowing continuous monitoring of the motor health. Although the method could be readily generalized, its presentation is limited in this paper to BLDC motors.

II. Rotor Fault Detection In Non-Stationary BLDC Motors

Potential faults in BLDC machines can be categorized as stator faults, rotor faults, bearing faults, and inverter faults. Rotor faults could be due to eccentricities, unbalanced rotors, damaged rotor magnets, misalignments, and asymmetries [8]. Rotor eccentricities occur when there is an unequal air-gap between the stator and the rotor and are classified into two main types: static and dynamic, with the latter being more severe of the two [1,9]. If the eccentricity were to become large, the resulting unbalanced radial forces could cause the stator and rotor to rub, resulting in damage to both the stator and the rotor. In the case of the static air-gap eccentricity, the position of the minimal radial air-gap length is fixed in space. In the case of dynamic eccentricity, the center of the rotor is not at the center of rotation, and the position of the minimum air-gap rotates with the rotor. Mechanically unbalanced rotors are usually caused by misaligned load. This unbalance causes slight dynamic eccentricity and motor vibration, eventually leading to motor bearing failure. Dynamic eccentricity and mechanically unbalanced rotors are used in this paper to develop the proposed detection method and illustrate its viability.

It is known that rotor defects such as a dynamic eccentricity can be detected by monitoring certain characteristic fault frequencies in the stator current of BLDC motors operating at constant speed [8]. These frequencies are given by

$$f_{rf} = f_e \pm k\frac{f_e}{P/2}, \tag{1}$$

where f_{rf} is the rotor fault frequency, f_e is the fundamental frequency, P is the number of poles in the BLDC machine, and k is any integer. These fault frequencies are also present when the current is non-stationary (dynamic motor operation). In such a case, the fault components change in frequency and magnitude depending on the operating point (speed and load) of the motor. These fault frequencies will be tracked continuously over time using the proposed algorithm.

III. Spectrogram and Windowed Fourier Ridges

A. Windowed Fourier Transform and Spectrogram

The windowed Fourier transform was developed by Gabor in 1946 when windowed Fourier atoms were introduced to measure the "frequency variations" of sounds. The windowed Fourier transform, *Sf* of a function *f(t)* is given by [10]

$$Sf(u,\xi) = \int_{-\infty}^{+\infty} f(t)\,g(t-u)\,e^{-i\xi t}dt, \tag{2}$$

where *g(t)* is a real and symmetric window translated by *u* and modulated by the frequency ξ. This transform is also called the short time Fourier transform (STFT) because the multiplication by *g(t-u)* localizes the Fourier integral in the neighborhood of $t = u$. The resolution in time and frequency of the STFT depends on the spread in time and frequency of the selected window type (Rectangle, Blackman, Hamming, Gaussian, Hanning, etc.). This spread is the smallest when the Gaussian window defined by (3) is used [10].

$$g(t) = e^{\left(-18t^2\right)}. \tag{3}$$

The STFT can be implemented digitally and efficiently in real-time using discrete Fourier transforms (DFT). The energy density possessed by the STFT is called a Spectrogram, denoted by P_Sf and is give by [10]

$$P_S f(u,\xi) = \left|Sf(u,\xi)\right|^2 = \left|\int_{-\infty}^{+\infty} f(t)\,g(t-u)\,e^{-i\xi t}dt\right|^2. \tag{4}$$

B. Windowed Fourier Ridges

The spectrogram measures the energy of *f(t)* in the time-frequency neighborhood of *(u,ξ)*. Windowed Fourier ridges are the local maxima of the spectrogram that represent the instantaneous frequencies. The instantaneous frequency of any function *f(t)* is defined as a positive derivative of the phase, $\omega(t) = \varphi'(t),\ t \geq 0$, where φ is the phase of *f(t)* [10]. If the signal *f(t)* has only one frequency component, then the instantaneous frequency is $\xi(t) = \varphi'(t)$, and the amplitude *a* can be calculated by

$$a(u) = \frac{2\left|Sf\left(u,\xi(u)\right)\right|}{\sqrt{s}\left|\hat{g}(0)\right|}, \tag{5}$$

where s is the length and $\hat{g}(\omega)$ is the Fourier transform of the window *g(t)* respectively. If $\Phi_S(u,\xi)$ is the complex phase of *Sf(u,ξ)*, then it can be shown that the ridge points are points of stationary phase [10]:

$$\frac{\partial\Phi_S(u,\xi)}{\partial u} = \varphi'(u) - \xi = 0. \tag{6}$$

The ridge algorithm thus computes the instantaneous frequencies of a signal *f(t)* from the local maxima of $P_Sf\,(u,\xi)$. This approach was introduced by Delprat et al. to analyze musical sounds [11].

Generally, the number of instantaneous frequencies is unknown. In such cases all local maxima of $P_Sf\,(u,\xi)$ which are also points of stationary phase are calculated. These points define curves in the *(u,ξ)* planes that are the ridges of the windowed Fourier transform. Ridges corresponding to a small amplitude are often removed because they can be artifacts of noise variations, or "shadows" of other instantaneous frequencies created by the side-lobes of $\hat{g}(\omega)$. The ridges will be distinct as long as the distance between any two

instantaneous frequencies satisfies (7), where $\Delta\omega$ is the bandwidth of the window [10].

$$\left|\varphi_1'(u)-\varphi_2'(u)\right| \geq \frac{\Delta\omega}{s}. \tag{7}$$

As the amplitudes of the rotor fault frequencies in the stator current of a defective BLDC motor are very small in comparison to the fundamental, the ridge algorithm would extract the fundamental frequency instead of the fault frequency. Hence, the stator current would have to be filtered to remove the fundamental and all other inverter harmonics prior to the application of the ridge algorithm.

To illustrate the concept, a test signal i_a approximating a rotor fault and having a fundamental of amplitude 0.05 A (corresponding to a filtered stator current) with two rotor fault sidebands of amplitude 0.07 A is generated using

$$\begin{aligned} i_a = {} & 0.05\cos\left(2\pi p(t)t\right)+0.07\cos\left(4\pi p(t)t/3\right) \\ & +0.07\cos\left(8\pi p(t)t/3\right). \end{aligned} \tag{8}$$

The three frequencies in (8) are the fundamental frequency *p(t)* and two rotor fault frequencies at 2/3rd and 4/3rd of the fundamental frequency *p(t)*. The amplitudes in (8) were chosen arbitrarily to imitate a rotor fault scenario as close as possible. The frequency *p(t)* is varied sinusoidally between 0 and 120 Hz. Fig. 2 shows the Fourier ridges (instantaneous frequencies) of the test signal extracted from the spectrogram computed using (4). The Wavelab802 toolbox for MATLAB from Stanford University is used to implement the windowed Fourier ridge algorithm [12]. The choice of a windowing function can play an important role in determining the quality of overall results. The main role of the window is to damp out the effects of the Gibbs phenomenon that results from truncation of an infinite series [13,14]. Different windows offer different trade offs between the ability to offer good frequency resolution and introduction of undesired artifacts (Gibbs phenomenon) [13,14]. A Gaussian window of length

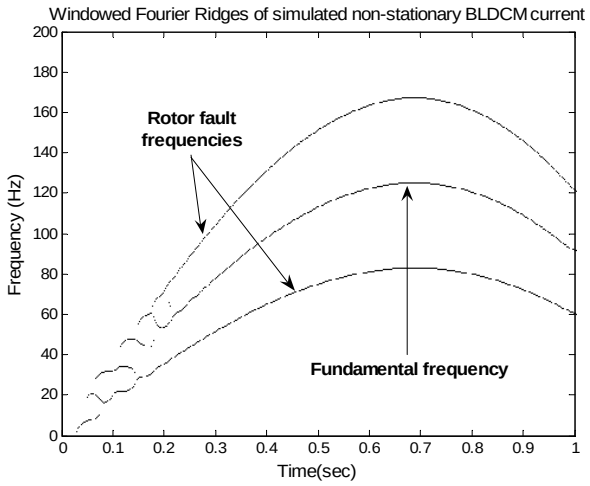

Figure 2. Windowed Fourier ridges of simulated non-stationary stator current in a faulty BLDC motor.

0.1 seconds is used in the present simulation example though other window types could be used. The length is chosen through trial and error to obtain a good frequency resolution while simultaneously maintaining time resolution. A larger window produces a smaller frequency resolution while not providing any significant improvement in the time resolution. Similarly, a smaller time window is found to provide a marginally improved frequency resolution while reducing the time resolution. The fault sideband ridges in Fig. 2 can be clearly seen to be tracked over time. The frequency resolution is reduced at very low frequencies and this is expected due to the small size of the window. The simulation demonstrates the feasibility of the approach, but also underscores possible limitations such as the choice of the size and type of the window. However, the method is robust and easy to implement in practice.

IV. Windowed Fourier Ridge Fault Detection Algorithm

A block schematic of the proposed algorithm is shown in Fig. 3. The proposed algorithm to monitor developing rotor faults in a BLDCM is as follows. Firstly, the fundamental and harmonics greater than two are adaptively filtered using an analog switch capacitor tracking filter. Next, a spectrogram is obtained from the filtered current signal using a Gaussian window as it provides the best frequency resolution among all windows. The ridge algorithm is then used to extract the instantaneous frequencies (ridges) from the local maxima of this spectrogram. A simple fault metric is then calculated by calculating the root mean square (RMS) value of the instantaneous amplitudes of the fault ridges. This metric is used to indicate a developing rotor fault. Thresholds can be set to determine the severity of the fault and provide an indication to the operator to take necessary precautionary action. Such thresholds can be set to vary with load and speed conditions.

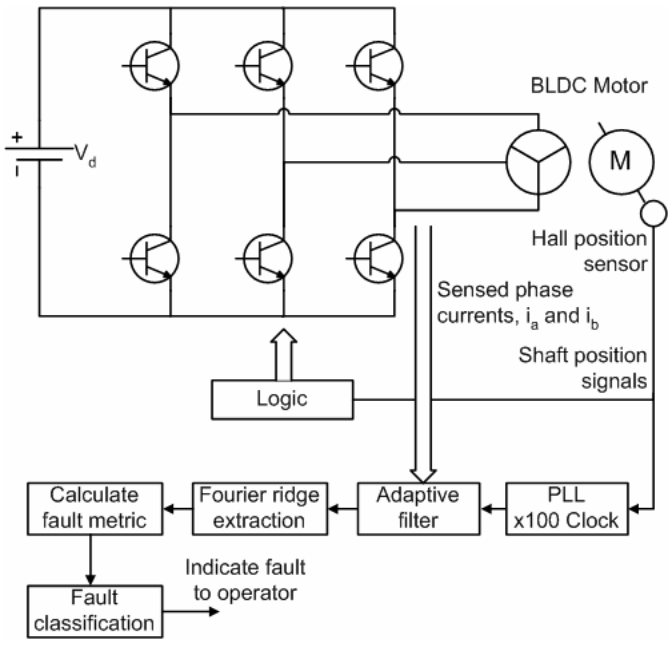

Figure 3. Rotor fault detection in BLDC motors using windowed Fourier ridge algorithm.

V. EXPERIMENTAL RESULTS

The experimental setup is shown in Fig. 4. A 12V, 1 kW, 6-pole BLDC motor with surface mount magnets is coupled to a DC generator that acts as a load. The BLDC motor is driven by an inverter which features an integrated current control loop. The inverter is supplied from a 12V deep cycle lead-acid battery. An analog speed controller designed at Georgia Institute of Technology is used to control speed. The speed signal is provided by a 1000 ppr optical encoder coupled to the DC generator. Hall Effect sensors are used to sense the motor stator currents. One of the phase currents is passed through the analog tracking filter. The filtered current as well as the raw input current is acquired using a 16-bit data acquisition system.

The analog tracking filter is a switch capacitor filter. The tracking filter removes the fundamental and all frequencies greater than two. The composition of the filter is shown in Fig. 5. The notch filter used to filter the fundamental is a 6^{th} order Elliptic switch capacitor filter designed using the software FilterCAD from Linear Technologies. The 6^{th} order filter is implemented using the LTC1061 high performance triple universal integrated circuit. The ratio of the 0dB width to the notch width is 10:1 with a notch attenuation of 56dB. A 8^{th} order Butterworth low pass switch capacitor filter is used to filter out all harmonics above the second harmonic. The low pass switch capacitor filter is implemented using a monolithic 8^{th} order filter chip MAX295 from Maxim. A low pass attenuation of well over 80dB is achieved. The MAX295 has an uncommitted operational amplifier that is used to finally amplify the filtered signal prior to data acquisition. The pass band ripple is limited to less than 100mdB. Pre-filters and post-filters are provided for anti-aliasing and clock-feed through removal. Clocking for the filter is obtained from the BLDC motor's Hall position sensors using a Phase Locked Loop (PLL) that tracks the fundamental frequency of current. The filter is fabricated on a 4-layer printed circuit board to obtain noise-free performance.

For a six-pole BLDC motor, the rotor fault frequencies occur at $1/3^{rd}$, $2/3^{rd}$, $4/3^{rd}$, and $5/3^{rd}$ times the fundamental frequency as computed from (1). Rapid time-varying motor operation is obtained by varying the speed reference. Experiments are conducted with sinusoidal, triangular, and randomly changing speed references. The sinusoidal and triangular references vary at a rate of 0 to 10 Hz representing most practically occurring applications. A signal generator is used to provide the sinusoidal and triangular reference signals. The motor speed varies in the range of 600 rpm to 1800 rpm. Two fault cases are presented here: a mechanically unbalanced rotor and a dynamic eccentricity.

A. Mechanically unbalanced rotor

A mechanically unbalanced rotor is implemented by mounting a slotted disk on the shaft of the motor (Fig. 4). The level of unbalance can be changed depending on the position of the bolt on slots in the disk. Such an unbalanced disk causes slight unbalance on the rotor shaft besides vibration and pulsating torques. An adaptive tracking filter with a 30 dB notch attenuation is used in this experiment to remove the fundamental frequency and all frequencies above the second harmonic.

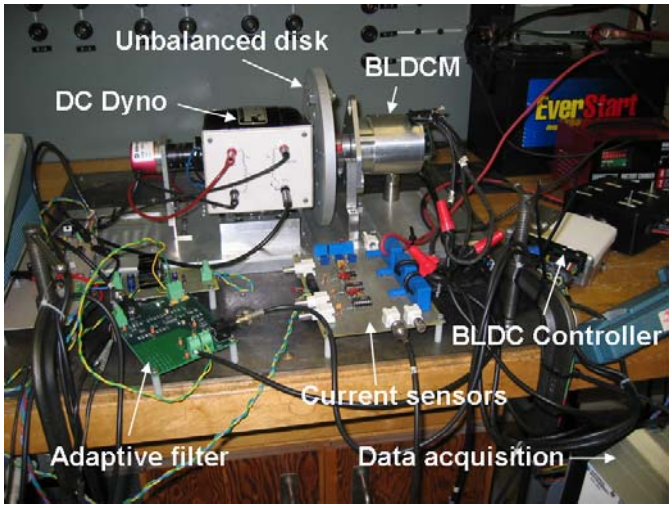

Figure 4. Experimental arrangement to test fault detection in dynamically operating BLDC motors.

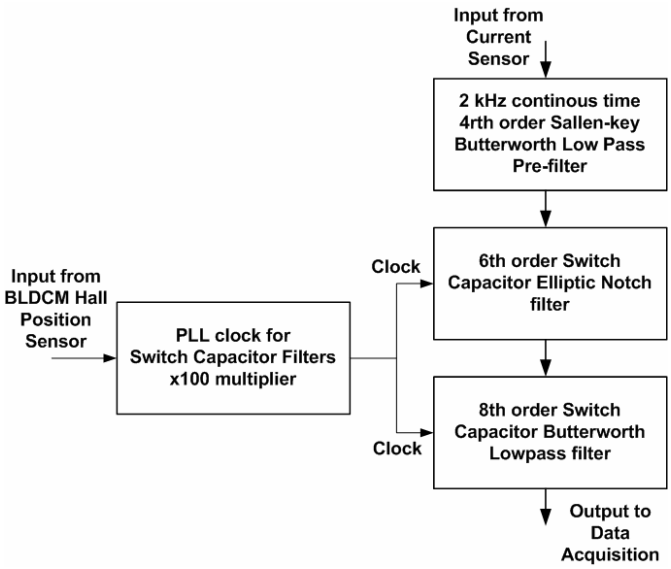

Figure 5. Block diagram of analog tracking filter.

A Gaussian window of length 0.25 seconds is used to compute the spectrogram. This length is chosen through trial and error to obtain the best compromise between frequency and time resolution. The stator current of a mechanically unbalanced BLDC motor (with bolt on one of the disk slots) operating with a 3 Hz sinusoidal speed reference is shown in Fig. 6. The corresponding spectrogram of the filtered stator current calculated using (4) is also shown in Fig. 6. The fault frequencies are still not distinctly visible as the spectrogram extracts all spectral components including noise from the filtered current. The instantaneous fault frequencies or fault ridges are now extracted from the local maxima of the spectrogram by testing all extracted maxima for stationary phase using (6). Thus only the fault ridges (instantaneous fault frequencies) are extracted from the filtered current and are shown in Fig. 7. A small fundamental component is also seen to be present in the extracted ridges of Fig. 7 as the 30dB tracking notch filter used here does not remove the fundamental frequency component completely.

The bolt on the disk is now removed to obtain a mechanically balanced motor and the experiment is repeated again with the same 3 Hz sinusoidal speed reference. The windowed Fourier ridges of the filtered current for this case are shown in Fig. 8. The segment of current shown is identical to the one used in Fig. 6. A small fundamental component is again seen to be present due to reasons mentioned earlier. As the disk even without the bolt comprises a slight unbalance by itself, some fault harmonic frequencies are seen, but these are smaller than the case with a bolt on the disk as shown previously in Fig. 7. Fig. 9 shows the fault metrics calculated for mechanically balanced and unbalanced motors using the instantaneous RMS of the fault ridge amplitudes (Figs. 7 and 8) extracted from the spectrogram of the filtered stator current. A clear change can be seen in the fault metric of the mechanically unbalanced motor indicating a fault condition. This fault metric can be used along with a predetermined threshold as an indicator for automatic detection of rotor faults in BLDC motors. More sophisticated fault classifiers using pattern recognition techniques can also be used if needed [15].

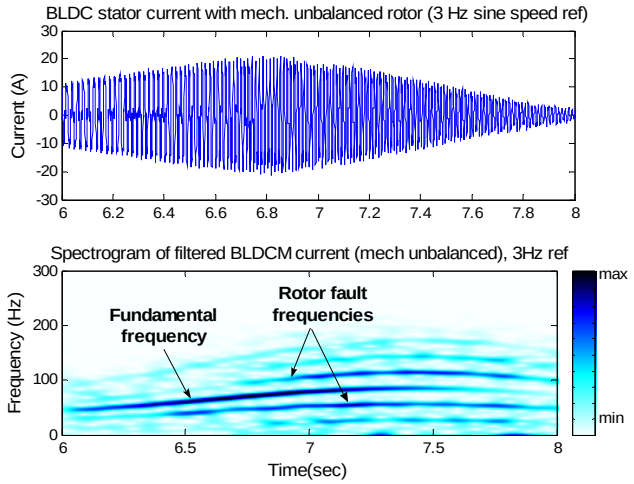

Figure 6. Non-stationary BLDC motor stator current and the spectrogram of the corresponding filtered BLDC motor (with mechanically unbalanced rotor) stator current with 3 Hz sine speed reference.

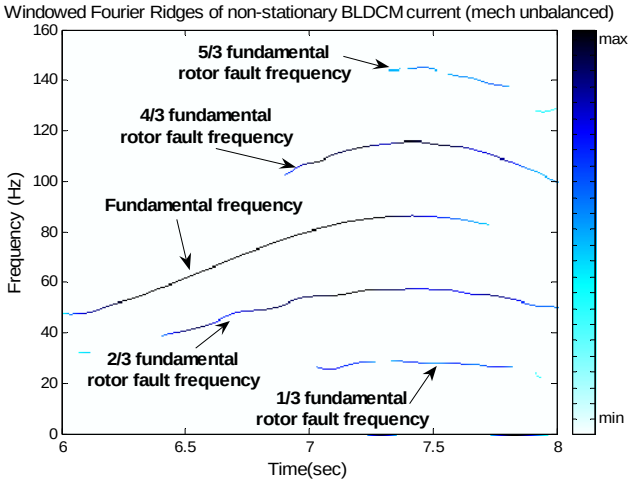

Figure 7. Windowed Fourier ridges of filtered BLDC motor (with mech. unbalanced rotor) stator current and 3 Hz sine speed reference.

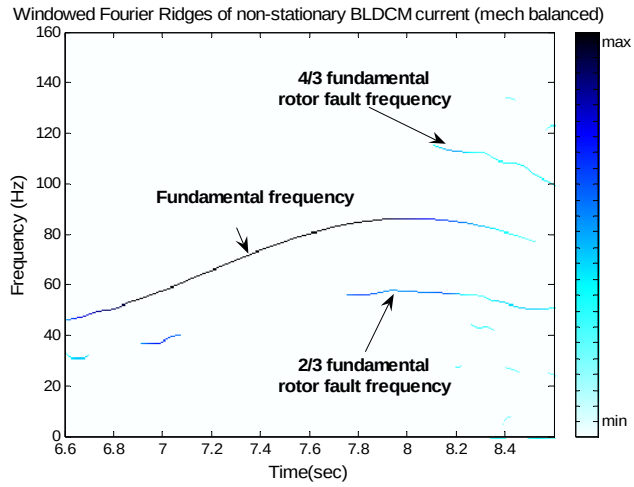

Figure 8. Windowed Fourier ridges of filtered BLDC motor (with mech. balanced rotor) stator current and 3 Hz sine speed reference.

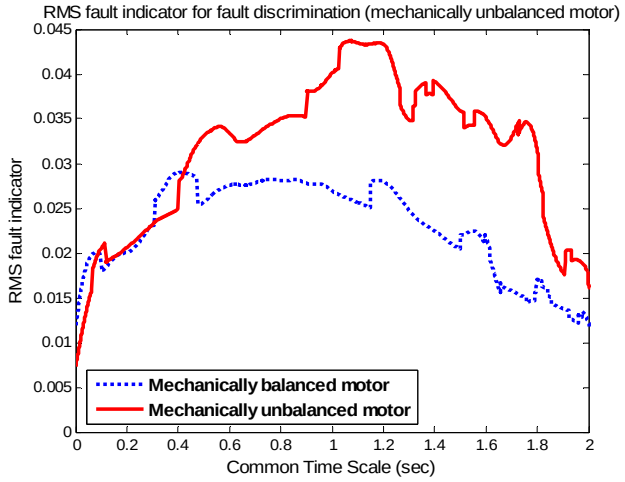

Figure 9. RMS fault indicator discriminates BLDC rotor unbalance (3 Hz sine speed ref).

B. *Dynamic Eccentricity*

As mentioned earlier, in dynamic eccentricity the center of the rotor is not at the center of the stator and the position of minimum air gap rotates with the rotor. This misalignment may be caused by several factors such as misalignment of bearings, mechanical resonance at critical speeds, a bent rotor shaft, or wear of bearings. An actual dynamic eccentricity is implemented in the laboratory. The rotor is first removed from the bearing. One side of the rotor shaft at one end of the motor is finely machined and then placed back onto the bearing. Shims are now inserted between the bearing and the shaft as shown in Fig. 10. The length of the air-gap being 0.75 mm, the rotor is shifted by approximately 0.25 mm (32% of normal air-gap length) from its center by inserting a steel shim of thickness 0.001 inches (~ 0.25 mm). The defect induced in this manner represents a realistic dynamic eccentricity fault that can occur during normal motor operation.

The windowed Fourier ridges (instantaneous fault frequencies) of the filtered stator current of a motor with

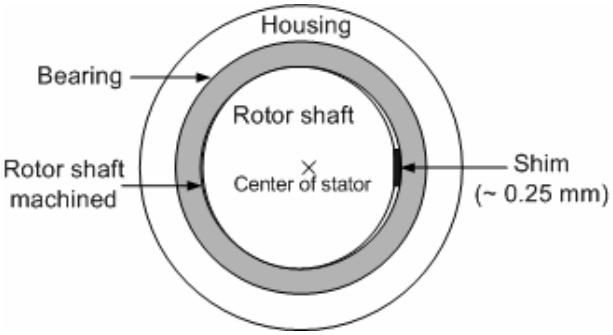

Figure 10. Laboratory implementation of dynamic eccentricity.

dynamic eccentricity operating with a 3 Hz sinusoidal speed reference is shown in Fig. 11. These Fourier ridges are extracted from the spectrogram of the filtered current signal computed using (4). A notch filter with an attenuation of 56 dB is used in this experiment. As the fundamental has been almost completely suppressed, the ridge algorithm detects and tracks only the fault frequencies. Again a Gaussian window of length 0.25 seconds is used in the experiments. The data is processed offline in MATLAB using the Wavelab802 toolbox. The fault frequencies are seen to be tracked over time. The windowed Fourier ridges for a faulty BLDC motor operating with a 6 Hz sinusoidal speed reference and an 8 Hz triangular speed reference are shown in Figs. 12 and 13. In both the cases the fault frequencies are again distinctly tracked over time.

To validate the effectiveness of the algorithm, the BLDC motor with dynamic eccentricity is then operated with a speed reference signal that changes randomly. The non-stationary stator current and the spectrogram of the filtered stator current computed using (4) are shown in Fig. 14. The spectrogram does not clearly depict the instantaneous fault frequencies in the filtered current signal. The windowed Fourier ridges are then extracted from the local maxima of the spectrogram. Fig. 15 shows the extracted fault ridges that are tracked distinctly over time. The extreme changes in the frequencies of the signal are now clearly visible. This demonstrates the effectiveness of the windowed Fourier ridge algorithm to track faults over all types of non-stationary conditions.

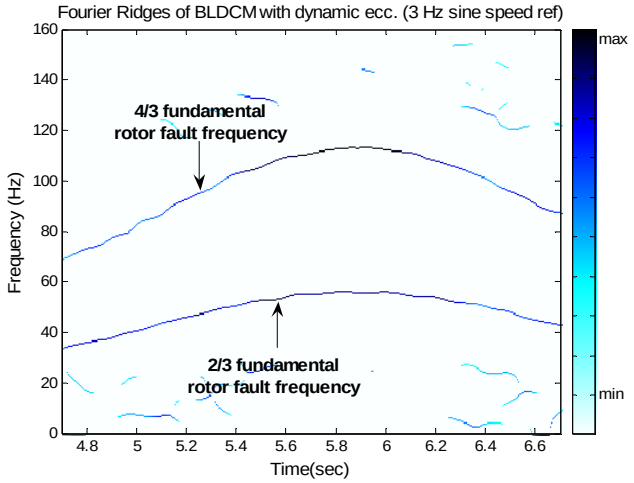

Figure 11. Windowed Fourier ridges of filtered BLDC motor (with dynamic eccentricity) stator current and 3 Hz sine speed reference.

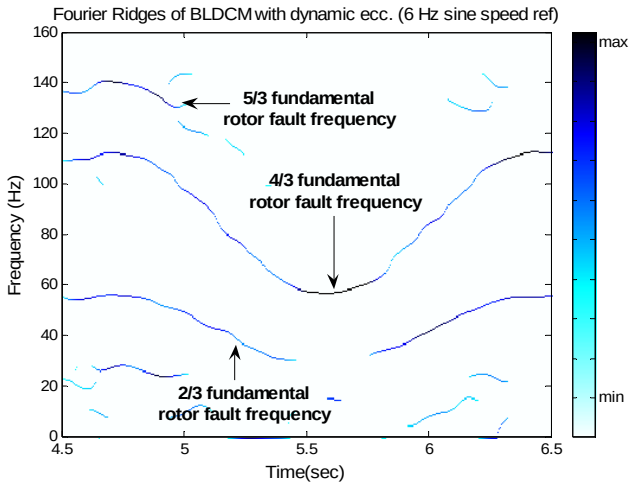

Figure 12. Windowed Fourier ridges of filtered BLDC motor (with dynamic eccentricity) stator current and 6 Hz sine speed reference.

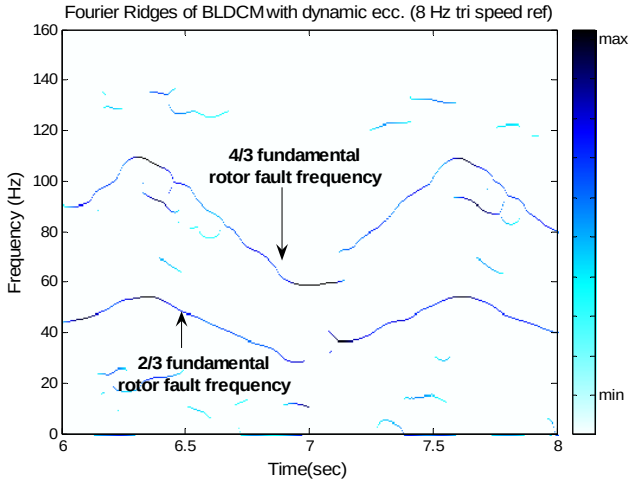

Figure 13. Windowed Fourier ridges of filtered BLDC motor (with dynamic eccentricity) stator current and 8 Hz triangular speed reference.

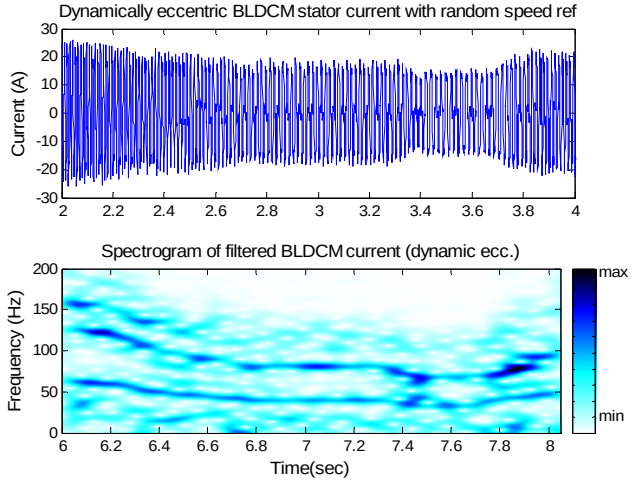

Figure 14. Non-stationary BLDC motor stator current and the spectrogram of the corresponding filtered BLDC motor (with dynamic eccnetricity) stator current with random speed reference.

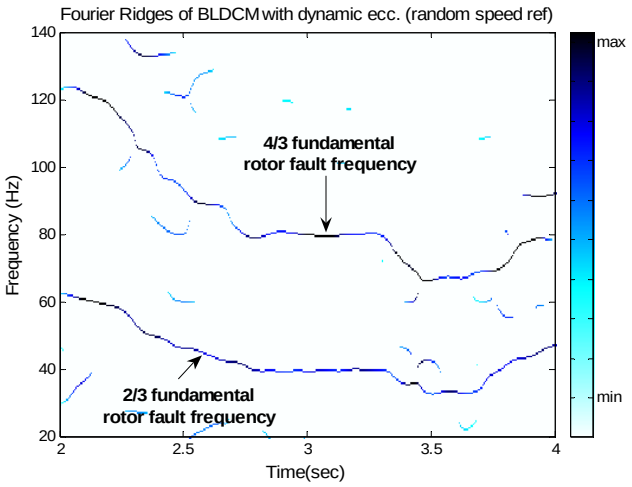

Figure 15. Windowed Fourier ridges of filtered BLDC motor (with dynamic eccentricity) stator current and random speed reference.

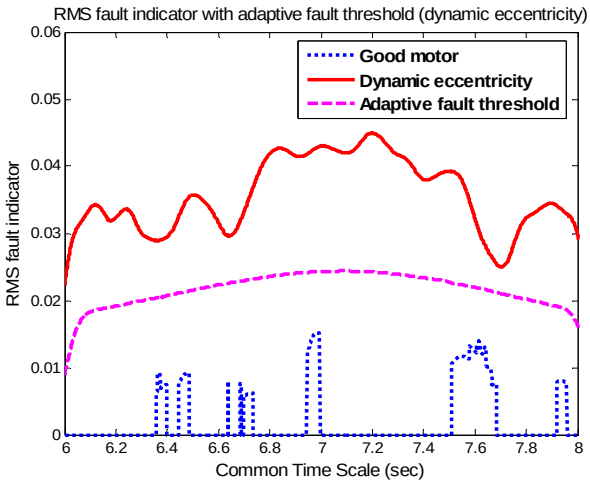

Figure 16. Detecting dynamic eccentricity with adaptive threshold set at 2% of fundamental amplitude (3 Hz sine speed reference).

During the experiments it is noted that the ridge algorithm is able to extract frequencies from the motor stator current up to a sinusoidal speed reference of 15 Hz and a triangular speed reference of 10 Hz. Beyond these speed reference rates, the current is extremely non-stationary (especially with a triangular reference) and no longer possess any instantaneous frequency. However such non-stationarity does not commonly occur in motor applications and any non-stationary fault detection method based on the windowed Fourier ridge algorithm should take into account the severity of the non-stationary behavior that may be encountered.

A simple fault metric is computed by calculating the RMS of the fault ridge amplitudes extracted from the spectrogram of the filtered stator current. The fault metric for a motor with dynamic eccentricity and a good motor are shown in Fig. 16. A significant difference in the fault metrics of the good and the faulty motor cases can be seen. The fault can be automatically detected by setting a threshold. An adaptive heuristic threshold that varies as 2% of the amplitude of the fundamental frequency is shown in Fig. 16. This threshold is unique to each application and each motor.

VI. Conclusions

A method of diagnostics of rotor faults in BLDC motors operating under continuous non-stationary operation is presented, perhaps for the first time, in this paper. The windowed Fourier ridge algorithm is proposed as a novel solution to this problem. Windowed Fourier ridges are the local maxima computed from the spectrogram of a non-stationary signal. The Fourier ridges can be detected for maxima of comparable magnitude in multi-component signals. The method is not limited to BLDC motors but can be applied to other motors as well.

The ability of the method to detect BLDC motor rotor faults namely unbalanced rotors and dynamic eccentricities in various cases of non-stationarity has been demonstrated. The windowed Fourier ridge algorithm is unfortunately dependent on the type and length of the window as it has to be chosen as a trade off between time and frequency resolution. However, the method is robust and is easy to implement in real-time. It is also computationally less intensive than other methods such as Wigner-Ville distributions. A simple fault metric based on the RMS of the extracted fault frequencies has been proposed for automatic fault detection. Although done here on a single test motor, we suggest that fault classification could be done using a threshold set heuristically or using sophisticated pattern recognition techniques such as artificial neural networks. This could be the subject of future investigations.

Acknowledgment

The authors wish to acknowledge the support of Delphi Corp., Troy, MI, and in particular the help of Dr. Tomy Sebastian (Delphi Saginaw Steering Systems), and Drs. Bruno Lequesne and Thomas W. Nehl (Delphi Research Labs), as well as financial support from the Duke Power Company in Charlotte, North Carolina.

References

[1] S. Nandi and H. A. Toliyat, "Condition monitoring and fault diagnosis of electrical machines – A review," in *Proceedings of the 34th Annual Meeting of the IEEE Industry Applications*, 1999, pp. 197-204.

[2] J. M. Cameron, W. T. Thomson, and A. B. Dow, Vibration and current monitoring for detecting airgap eccentricity in large induction motors," *IEE Proceedings*, vol. 133, pt. B, no. 3, 1986, pp.155-163.

[3] G. B. Kliman and J. Stein, "Methods of motor current signature analysis," *Electric Machines and Power Systems*, vol. 20, no. 5, 1992, pp. 463-474.

[4] B. Yazici and G. B. Kliman, "An adaptive statistical time-frequency method for detection of broken bars and bearing faults in motors using stator current," *IEEE Trans. Industry Applications*, vol.35, no. 2, 1999, pp. 442-452.

[5] K. Kim and A. G. Parlos, "Induction motor fault diagnosis based on neuropredictors and wavelet signal processing," *IEEE/ASME Trans. Mechatronics*, vol. 7, no. 2, 2002, pp. 201-219.

[6] R. Burnett, J. F. Watson, and S. Elder, "The application of modern signal processing techniques for use in rotor fault detection and location within three-phase induction motors," in *Proceedings of the 1995 IEEE Instrumentation and Measurement Technology Conference (IMTC/95)*, 1995, pp. 426-431.

[7] L. Eren and M. J. Devaney, "Motor bearing damage detection via wavelet analysis of the starting current transient," in *Proceedings of the*

18th IEEE Instrumentation and Measurement Technology Conference (IMTC 2001), 2001, pp. 1797-1800.

[8] S. Rajagopalan, W. le Roux, R.G. Harley and T.G. Habetler, "Diagnosis of potential rotor faults in brushless DC machines," in *Proceedings of the Second International Conference on Power Electronics, Machines and Drives (PEMD 2004)*, 2004, pp. 668-673.

[9] D. G. Dorell, W. T. Thomson, and S. Roach, "Analysis of airgap flux, current, and vibration signals as a function of the combination of static and dynamic airgap eccentricity in 3-phase induction motors," *IEEE Trans. on Industry Applications*, vol. 33, no. 1, 1997, pp.24-34.

[10] S. Mallat, *A Wavelet Tour of Signal Processing*, Academic Press, CA: 1999, p. 84-88, 102-107.

[11] N. Delprat, B. Escudie, P. Guillemain, R. Kroland-Martinet, P. Tchamitchian, and B. Torresani, "Asymptotic wavelets and Gabor analysis: Extraction of instantaneous frequencies," *IEEE Trans. on Information Theory*, vol. 3, 1992, pp. 644-664.

[12] *WaveLab802*, http://www-stat.stanford.edu/~wavelab.

[13] A. V. Oppenheim, R. W. Schafer, and J. R. Buck, *Discrete-Time Signal Processing*, Prentice Hall, 1999.

[14] L. R. Rabiner and B. Gold, *Theory and Application of Digital Signal Processing*, Englewood Cliffs, NJ: Prentice-Hall, Inc., 1975.

[15] X. Huang, T. G. Habetler, and R. G. Harley, "Detection of rotor eccentricity faults in closed-loop drive-connected induction motors using an artificial neural network," in *Proceedings of the IEEE Power Electronics Specialist Conference 2004 (PESC'04)*, 2004.

Paper Information

This paper was presented at the **Industry Applications Society 40th Annual Meeting (IEEE IAS2005),** Hong Kong on October 3, 2005 in Session 1 – Diagnostics.

Author information:

Satish Rajagopalan
W312 Van Leer Electrical Engineering Building
Georgia Institute of Technology
777 Atlantic Dr. NW
Atlanta, Georgia 30332, USA
Phone: 404 894 5563
rsatish@ece.gatech.edu

Thomas G. Habetler (Corresponding Author)
E171 Van Leer Electrical Engineering Building
Georgia Institute of Technology
777 Atlantic Dr. NW
Atlanta, Georgia 30332, USA
Phone: 404 894 9829
Fax: 404 894 4641
thabetler@ece.gatech.edu

Ronald G. Harley
E171 Van Leer Electrical Engineering Building
Georgia Institute of Technology
777 Atlantic Dr. NW
Atlanta, Georgia 30332, USA
Phone: 404 894 1876
Fax: 404 894 4641
ron.harley@ece.gatech.edu

José M. Aller
Universidad Simón Bolívar
Caracas 1080A, VENEZUELA
jaller@usb.ve

José A. Restrepo
Universidad Simón Bolívar
Caracas 1080A, VENEZUELA
restrepo@usb.ve